




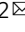

| | |
|--------------|---|
| Title | A boron-transfer mechanism mediating the thermally induced revival of frustrated carbene-borane pairs from their shelf-stable adducts |
| Author(s) | Hoshimoto, Yoichi; Sakuraba, Mahiro; Kinoshita, Takuya et al. |
| Citation | Communications Chemistry. 2021, 4(1), p. 137 |
| Version Type | VoR |
| URL | https://hdl.handle.net/11094/92549 |
| rights | This article is licensed under a Creative Commons Attribution 4.0 International License. |
| Note | |

The University of Osaka Institutional Knowledge Archive : OUKA

<https://ir.library.osaka-u.ac.jp/>

The University of Osaka

A boron-transfer mechanism mediating the thermally induced revival of frustrated carbene–borane pairs from their shelf-stable adducts

Yoichi Hoshimoto¹, Mahiro Sakuraba¹, Takuya Kinoshita¹, Masaki Ohbo², Manussada Ratanasak², Jun-ya Hasegawa² & Sensuske Ogoshi¹

Chemists have designed strategies that trigger the conformational isomerization of molecules in response to external stimuli, which can be further applied to regulate the complexation between Lewis acids and bases. We have recently developed a system in which frustrated carbene–borane pairs are revived from shelf-stable but external-stimuli-responsive carbene–borane adducts comprised of *N*-phosphine-oxide-substituted imidazolylienes (Poxlms) and triarylboranes. Herein, we report the detailed mechanism on this revival process. A thermally induced borane-transfer process from the carbene carbon atom to the *N*-phosphinoyl oxygen atom initiates the transformation of the carbene–borane adduct. Subsequent conformational isomerization via the rotation of the *N*-phosphinoyl group in Poxlm moieties eventually leads to the revival of frustrated carbene–borane pairs that can cleave H₂. We believe that this work illustrates an essential role of dynamic conformational isomerization in the regulation of the reactivity of external-stimuli-responsive Lewis acid–base adducts that contain multifunctional substituents.

¹Department of Applied Chemistry, Faculty of Engineering, Osaka University, Osaka, Japan. ²Institute for Catalysis, Hokkaido University, Sapporo, Japan.
✉email: hoshimoto@chem.eng.osaka-u.ac.jp; hasegawa@cat.hokudai.ac.jp; ogoshi@chem.eng.osaka-u.ac.jp

There have been many recent developments in the chemistry of frustrated Lewis pairs (FLPs) that have been of note, for example, the activation of H_2 mediated by main-group elements^{1–9}. In general, FLPs are transient and not shelf-stable species making their isolation challenging. Meanwhile, chemists have developed strategies that trigger the conformational isomerization of molecules in response to external-stimuli^{10–13}. These strategies can also be used to generate transient FLP species from classical Lewis adducts (CLAs) that act like their shelf-stable precursors^{14–26}. In 2015, we demonstrated a strategy to generate FLPs from shelf-stable CLAs (**PoxIm-B¹** in Fig. 1) that are comprised of *N*-phosphine-oxide-substituted imidazolylienes (**PoxIm**s; **1**) and $B(C_6F_5)_3$ (**B¹**). Here, the revival of the FLP from the CLA is closely controlled by a thermally induced conformational isomerization of the *N*-phosphinoyl moiety^{17,27–30}. In 2018, Stephan et al. reported a system to control the generation of FLPs from CLAs via a light-induced *E/Z* isomerization of $(C_6F_5)_2B(p-Tol)S(C) = CCH(tBu)$ ³¹. Nevertheless, such FLP revival systems, including external-stimuli-responsive conformational isomerizations, are still underdeveloped. Thus, clarifying the relationship between external-stimuli-responsive conformational isomerizations and the interconversion that occurs between frustrated and quenched Lewis pairs is of great importance. This would allow a significant expansion of different strategies to design and apply FLP species¹⁹.

In our system that uses **PoxIm**s, the revival mechanism has not been fully explained. A tentative mechanism in which a $B(C_6F_5)_3$ moiety is repelled by the *N*-phosphinoyl group via a thermally induced isomerization from the *syn* to *anti* conformation had been proposed. In this case, the *syn/anti* conformation refers to the relative orientation of the carbene carbon atom and the *N*-phosphinoyl oxygen atom with respect to the N–P bond (Fig. 1a)¹⁷. Herein, we report the results of a combined experimental and theoretical mechanistic study that demonstrates the key role of a transfer step where the triarylborane (BAR_3) unit on the carbene carbon atom moves to the *N*-phosphinoyl oxygen atom (Fig. 1b). In this study, **PoxIm**s with 2,6-*i*Pr₂-C₆H₃, 2,4,6-Me₃-C₆H₂, and 3,5-*t*Bu₂-C₆H₃ groups were studied and are herein referred to as **1a**, **1b**, and **1c**, respectively.

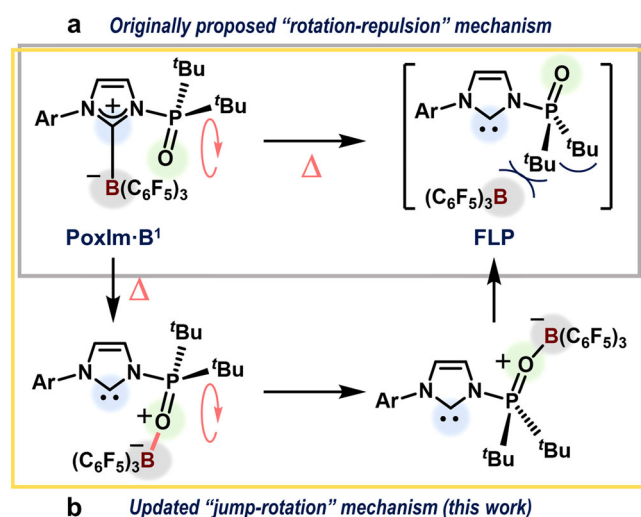


Fig. 1 Revival of FLPs from **PoxIm-B¹** adducts, induced by thermally responsive molecular motions. **a** A previously proposed mechanism. **b** The updated mechanism proposed based on the results of this work.

Results and discussion

Effects of Lewis acidity. To explore the impact of the Lewis acidity of BAR_3 on the formation and reactivity of the carbene–borane adducts, the reaction between **1a** and $B(p-HC_6F_4)_3$ (**B²**) was undertaken (Fig. 2a). Full consumption of **1a** was confirmed after 20 min, resulting in the formation of two CLAs, i.e., **2aB²**, which contains a *N*-phosphinoyl oxygen–boron bond, and **3aB²**, which contains a carbene–boron bond, in 61% and 29% yield, respectively. Previously, we have reported that, even at $-30^\circ C$, **2aB¹** could be converted to **3aB¹** and that full identification of **2aB¹** could therefore be achieved using NMR analysis conducted at $-90^\circ C$ ¹⁷. In the present case, **2aB²** exhibited a longer life-time at room temperature than **2aB¹**, which enabled us to prepare single crystals of **2aB²** by recrystallization from the reaction mixture at $-30^\circ C$. The molecular structure of **2aB²** was unambiguously confirmed using single-crystal X-ray diffraction (SC-XRD) analysis. A set of (*R_a*) and (*S_a*) atropisomers of **2aB²** was identified in the asymmetric unit of the single crystal. The molecular structure of (*R_a*)-**2aB²** is shown in Fig. 2b and demonstrates a rare example of complexation-induced N–P axial chirality²⁹. As the reaction progressed, **2aB²** was converted to **3aB²** and **4a**; **2aB²** was fully consumed within 6 h to afford these compounds in 75% and 25% yield, respectively. It should be noted that **4a** is likely furnished via the migration of the *N*-phosphinoyl group from the nitrogen atom to the carbene carbon atom. However, in the absence of **B²**, this migration only proceeded to 9% at $100^\circ C$, even after 25 h³⁰. The formation of **4a** was therefore promoted by the enhancement of the electrophilicity of the P center via the coordination of the *N*-phosphinoyl moiety to **B²**. Regeneration of **B²** was observed along with the production of **4a**. The molecular structure of **3aB²** was also confirmed by SC-XRD analysis (Fig. 2c). Comparison of the structural parameters between the solid-state structures of **3aB²** and **3aB¹** shows their similarity. For example, the C1–B distances in **3aB²** and in **3aB¹** are 1.710(3) Å and 1.696(3) Å, respectively. The interatomic distance of 3.257(3) Å between the O and B atoms in **3aB²** suggests the absence of a specific interaction between these atoms, similar to that in **3aB¹** (3.234(3) Å).

Thermolysis of **3aB²** at $60^\circ C$ for 3 h resulted in the generation of **4a** and **B²** in 77% and 73% yield, respectively, with concomitant formation of $[1a-H][HO(B^2)_2]$ in 4% yield (conversion of **3aB²** = 81%; Fig. 3a). Although **2aB²** was not observed via NMR analysis of this reaction at $60^\circ C$, the formation of **4a** and **B²** indicates the in situ regeneration of **2aB²** (*vide supra*). The formation of $[1a-H][HO(B^2)_2]$ can be rationalized in terms of a reaction between contaminated H_2O and the FLP species regenerated from **3aB²** via **2aB²**. The regeneration of the FLP species from **3aB²** was then clearly confirmed by treating **3aB²** with H_2 (5 atm) at $22^\circ C$, resulting in the formation of $[1a-H][H-B^2]$ (**5aB²**) in 19% yield with concomitant formation of $[1a-H][HO(B^2)_2]$ (8%) and **1a** (6%) (Fig. 3b). Under identical conditions, no reaction occurred when **3aB¹** was used¹⁷. At $60^\circ C$, **5aB²** was generated in 90% yield after 3 h, which is almost comparable with the production of **5aB¹** (89%) from **3aB¹**. Thus, the lower Lewis acidity of **B²** relative to **B¹** allowed a more facile revival of the FLP species from **3aB²** than from **3aB¹**. However, the lower Lewis acidity did not affect the progress of the heterolytic cleavage of H_2 by FLPs at $60^\circ C$.

Kinetic studies. To gain further insight into the reaction mechanism, the initial rate constants for the generation of **5aB¹**, k_{int} [$10^{-5} s^{-1}$], from the reaction between **3aB¹** and H_2 in 1,2-dichloroethane-*d*₄ (DCE-*d*₄) at $60^\circ C$ were estimated by varying the H_2 pressure from 0.5 to 5.0 atm (Fig. 4a). It should be noted here that when H_2 was pressurized at 5.0 atm, an excess of H_2 (ca.

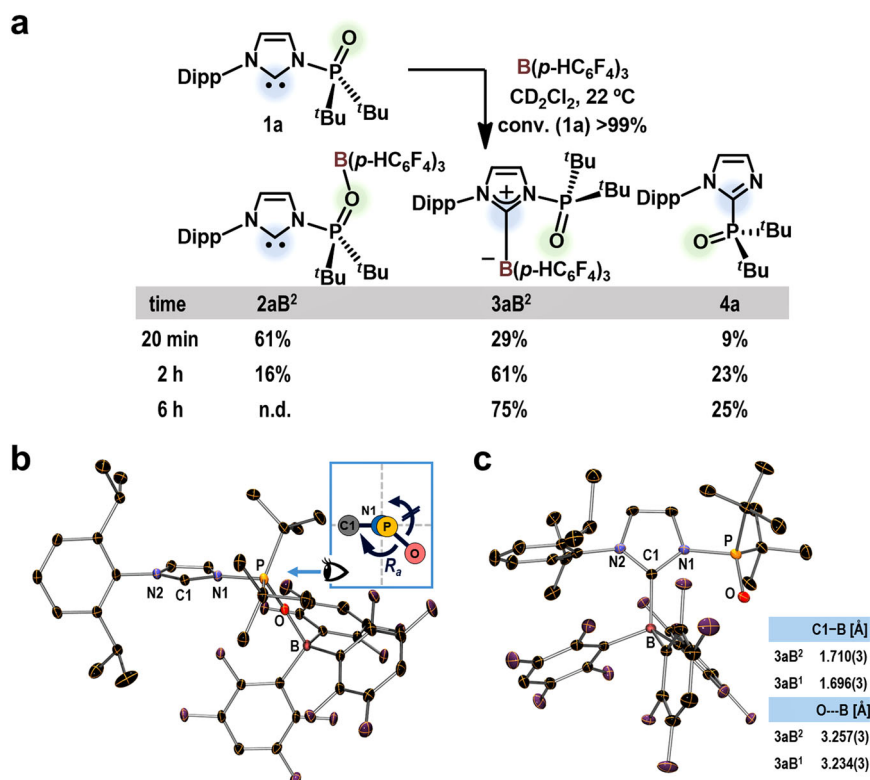


Fig. 2 Reaction between 1a and B(p-HC₆F₄)₃ (B²). **a** The reaction was monitored by NMR spectroscopy and the product yields were estimated based on ³¹P NMR analyses. **b** Molecular structure of (*R_a*)-2aB² with thermal ellipsoids at 30% probability; H atoms and solvated C₇H₈ molecules are omitted for clarity. Selected bond lengths [Å] and angles [°]: O–B 1.556(2), N1–P 1.707(2), P–O 1.513(1); P–O–B 165.2(1), C1–N1–P–O 128.0(1). **c** Molecular structure of 3aB² with thermal ellipsoids at 30% probability; H atoms are omitted for clarity. For comparison with 3aB¹ (cf. ref. ¹⁷), the carbene–boron bond lengths and interatomic distances between oxygen and boron atoms are shown; C1–N1–P–O: 15.3(2)°.

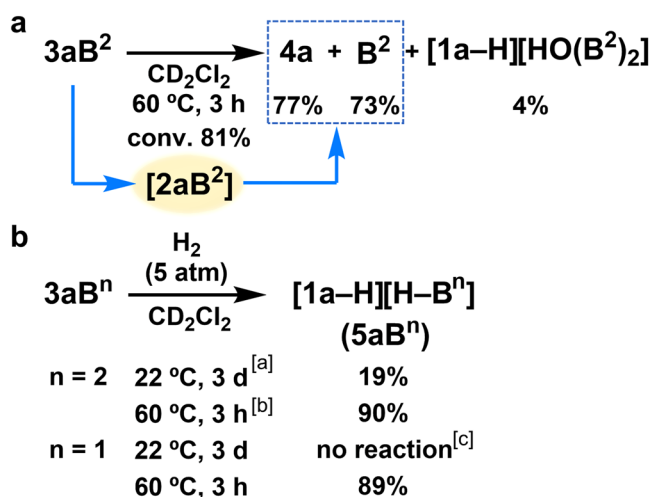


Fig. 3 Reactivity of carbene–borane adducts 3aBⁿ (n = 1, 2). **a**

Thermolysis of 3aB² monitored via NMR spectroscopy. Product yields were calculated based on ³¹P and ¹⁹F NMR analyses. **b** Reaction between 3aBⁿ and H₂. Product yields were calculated based on ¹⁹F and ³¹P analysis. ^a[1a–H][HO(B²)₂] and 1a were also observed in 8% and 6% yield, respectively. ^b[1a–H][HO(B²)₂] was also observed in 7% yield. ^cResults obtained using 3aB¹ are reproduced from ref. ¹⁷.

0.3 mmol) with respect to 3aB¹ (0.010 mmol) was added to the pressure-tight NMR tube. The concentration of H₂ clearly influenced the progress of the reaction, suggesting that the heterolytic cleavage of H₂ by the FLP species is involved in the rate-determining events. Next, the reaction between 3aB¹ and H₂ at

5.0 atm of pressure was monitored in DCE-*d*₄ whilst the temperature was varied from 50 to 80 °C (Supplementary Figure 27). Pseudo-first order rate constants, *k*_{obs} [10^{–5} s^{–1}], of 2.95(2), 11.2(8), 46.4(4) and 183(2) were estimated for the reactions at 50, 60, 70, and 80 °C, respectively. Thus, the activation energy and pre-exponential factor obtained from the plot based on the Arrhenius equation, ln*k*_{obs} = –(*E_a*/R)(1/*T*) + ln*A*, are *E_a* = 31.2 [kcal mol^{–1}] and *A* = 3.3(36) × 10¹⁶ [s^{–1}] (Fig. 4b). Given the close relation between *E_a* and Δ*H*[‡], the values obtained for *E_a* suggest that the formation of 5aB¹ via the reaction between 3aB¹ and H₂ only occurs at temperatures higher than 25 °C³².

Based on the results presented here and those previously reported¹⁷, the reaction between the carbene–borane adducts and H₂ to give [PoxIm–H][H–BAR₃] likely proceeds via the heterolytic cleavage of H₂ by the FLP species that are formed following the regeneration of the *N*-phosphinoyl oxygen–borane adducts. These steps are expected to be the rate-determining events because the concentration of H₂ (Fig. 4a), the steric bulk of the *N*-aryl group¹⁷ and the Lewis acidity of the BAR₃ moiety (Fig. 3b) influence the reaction rates and/or the temperature required to initiate the reaction between the carbene–borane adducts and H₂.

Theoretical studies. Density-functional theory (DFT) calculations were carried out at the ωB97X-D/6-311G(d,p), PCM (DCE)//ωB97X-D/6-31G(d,p) for H₂ and 6-31G(d) for all other atoms level of theory (Fig. 5a). The relative Gibbs free energies with respect to [1a + B¹] (0.0 kcal·mol^{–1}) are shown. During the transformation of 3aB¹ (–17.2 kcal·mol^{–1}) to 2aB¹ (–9.8 kcal·mol^{–1}), both of which were experimentally confirmed, the formation of an intermediate 2a'B¹ (–7.7 kcal·mol^{–1}) was predicted via a C-to-O transfer of B¹ in 3aB¹. This distinctive boron-transfer process takes place via saddle

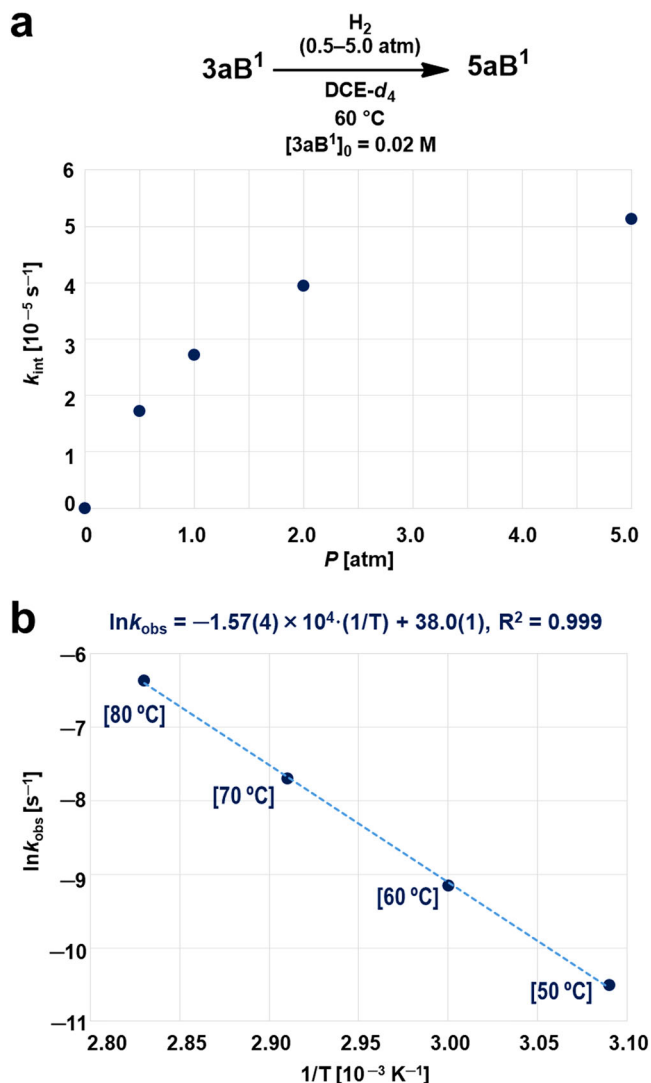


Fig. 4 Kinetic studies for the reaction between $3aB^1$ and H_2 . **a** Plot of the H_2 pressure, P [atm], as a function of the initial reaction rate constants, k_{int} [10^{-5} s^{-1}]. **b** Plot of $1/T$ [10^{-3} K^{-1}] as a function of $\ln k_{obs}$ [s^{-1}]. The k_{obs} values are the pseudo-first order rate constants for the formation of $5aB^1$ obtained from the reaction of $1a$ ($2.0 \times 10^{-2} \text{ M}$ in DCE- d_4) and H_2 (5 atm).

point **TS1a** (+7.3 kcal·mol⁻¹), while the potential energy surface around **TS1a** is very flat (Supplementary Figure 34 for details). The subsequent rotation of the *N*-phosphinoyl moiety via **TS2a** (+7.5 kcal·mol⁻¹) affords **2aB¹**. Next, the dissociation of the B–O bond occurs to regenerate [**1a** + **B¹**]. The optimized molecular structures of **TS1a** and **2aB¹** are shown in Fig. 5c. In **TS1a**, the interatomic distances C1...B and O...B are 4.24 and 3.34 Å, respectively, while **B¹** adopts a planar geometry. Thus, **B¹** is dissociated from both the carbene carbon and phosphinoyl oxygen atoms in **TS1a**, while the formation of the O–B bond (1.59 Å) is confirmed in **2aB¹**. Based on the quantum theory of atoms in molecule (AIM) method, neither bond paths nor bond critical points were confirmed between the B and C1/O atoms in **TS1a** (Supplementary Figure 37)^{33,34}. This AIM analysis demonstrates that several non-covalent interactions, including π – π and H...F interactions, exist between the **1a** and **B¹** moieties to stabilize **TS1a**.

Two plausible mechanisms were evaluated for the FLP-mediated cleavage of H_2 on the basis that the Lewis-basic center reacts with H_2 via cooperation with **B¹** (Fig. 5b). One possibility is that the carbene carbon atom works as a Lewis base (path I; the

right path in Fig. 5b)^{1–9,35,36}, while the other is that the *N*-phosphinoyl oxygen functions as a Lewis base (path II; the left path in Fig. 5b)³⁷. In path I, the heterolytic cleavage of H_2 takes place via **TS4a** (+11.4 kcal·mol⁻¹), which arises from the insertion of H_2 into the reaction field around the carbene carbon and boron atoms in **FLP-1aB¹**, affording **5aB¹** (–34.8 kcal·mol⁻¹), a species more thermodynamically stable than **3aB¹**. In the optimized structure of **TS4a** (Fig. 5d), the dissociation of the H1–H2 bond (H1...H2 = 0.84 Å) occurs with the partial formation of the H2–C1/H1–B bonds (H2...C1 = 1.83 Å/H1...B = 1.49 Å). Based on these results, the overall path from **3aB¹** to **5aB¹** via **FLP-1aB¹** is substantially exothermic ($\Delta G^\circ = -17.6 \text{ kcal}\cdot\text{mol}^{-1}$) and includes an overall activation energy barrier of +28.6 kcal·mol⁻¹ required to overcome **TS4a**. In path II, which takes place via **TS5a** (a transition state for the insertion of H_2 into the O–P bond) and **TS6a** (a transition state for the cleavage of H_2 between the O and P atoms), a higher activation energy barrier of +32.7 kcal·mol⁻¹ is predicted to yield intermediate **8aB¹**, which contains a P=O–H⁺ and B–H[–] species. It should be noted that the potential energy of the optimized **TS6a** (–3633.288355 hartree) is almost identical to that of the optimized **7aB¹** (–3633.288363 hartree), which causes the reversed Gibbs energy levels as shown in Fig. 5b after the Gibbs energy correction and implementation of solvent effect. Therefore, the discussion on the activation energy barrier to overcome **TS6a** from **7aB¹** should be not essential. The subsequent transfer of H⁺ from the *N*-phosphinoyl oxygen atom to the carbene carbon atom furnishes **5aB¹**, although the details of this process remain unclear at this point. The molecular structure of **TS6a** shows that the cleavage of the H1–H2 bond (H1...H2 = 0.85 Å) by the *N*-phosphinoyl oxygen and boron atoms occurs in a cooperative fashion (Fig. 5d). Given the experimental and theoretical results reported here, we conclude that path I is the more likely one.

The impact of the *N*-aryl substituents on the activation energy barriers for the regeneration of [**1** + **B¹**] was evaluated using calculations on **3bB¹**, which contains an *N*-2,4,6-Me₃-C₆H₂ group, as well as **3cB¹**, which contains an *N*-3,5-^{*i*}Bu₂-C₆H₃ group. This afforded ΔG^\ddagger values of +28.3 and +32.8 kcal·mol⁻¹ for **3bB¹** and **3cB¹**, respectively (Fig. 5a). These results are consistent with the experimental observations, i.e., that **3aB¹**–**3cB¹** did not react in the presence or absence of H_2 under ambient conditions under the applied conditions. Furthermore, these results might rationalize the fact that temperature to induce the reaction between these CLAs and H_2 increases in the order **3aB¹** (60 °C) < **3bB¹** (80 °C) < **3cB¹** (120 °C)¹⁷.

Conclusion. In summary, the reaction mechanism for the revival of frustrated carbene–borane pairs from external-stimuli-responsive classical Lewis adducts (CLAs), comprised of *N*-phosphine-oxide-substituted imidazolyldene (PoxIm) and triarylboranes (BAR₃), is reported based on a combination of experimental and theoretical studies. Remarkably, a transfer of the borane moiety from the carbene carbon atom to the *N*-phosphinoyl oxygen atom was identified as a key step in the heterolytic cleavage of H_2 by the regenerated FLP species. The optimized transition-state structure for this borane-transfer process was confirmed to include no bonding interactions between the carbene carbon/phosphinoyl oxygen and boron atoms, albeit that it is stabilized by intermolecular non-covalent interactions between the PoxIm and BAR₃ moieties. The heterolytic cleavage of H_2 takes place via the cooperation of the carbene carbon and the boron atoms, and exhibits a lower overall activation energy barrier than that of the path in which a combination of the *N*-phosphinoyl oxygen and boron atom mediates the H_2 cleavage. These results demonstrate the essential role of dynamic

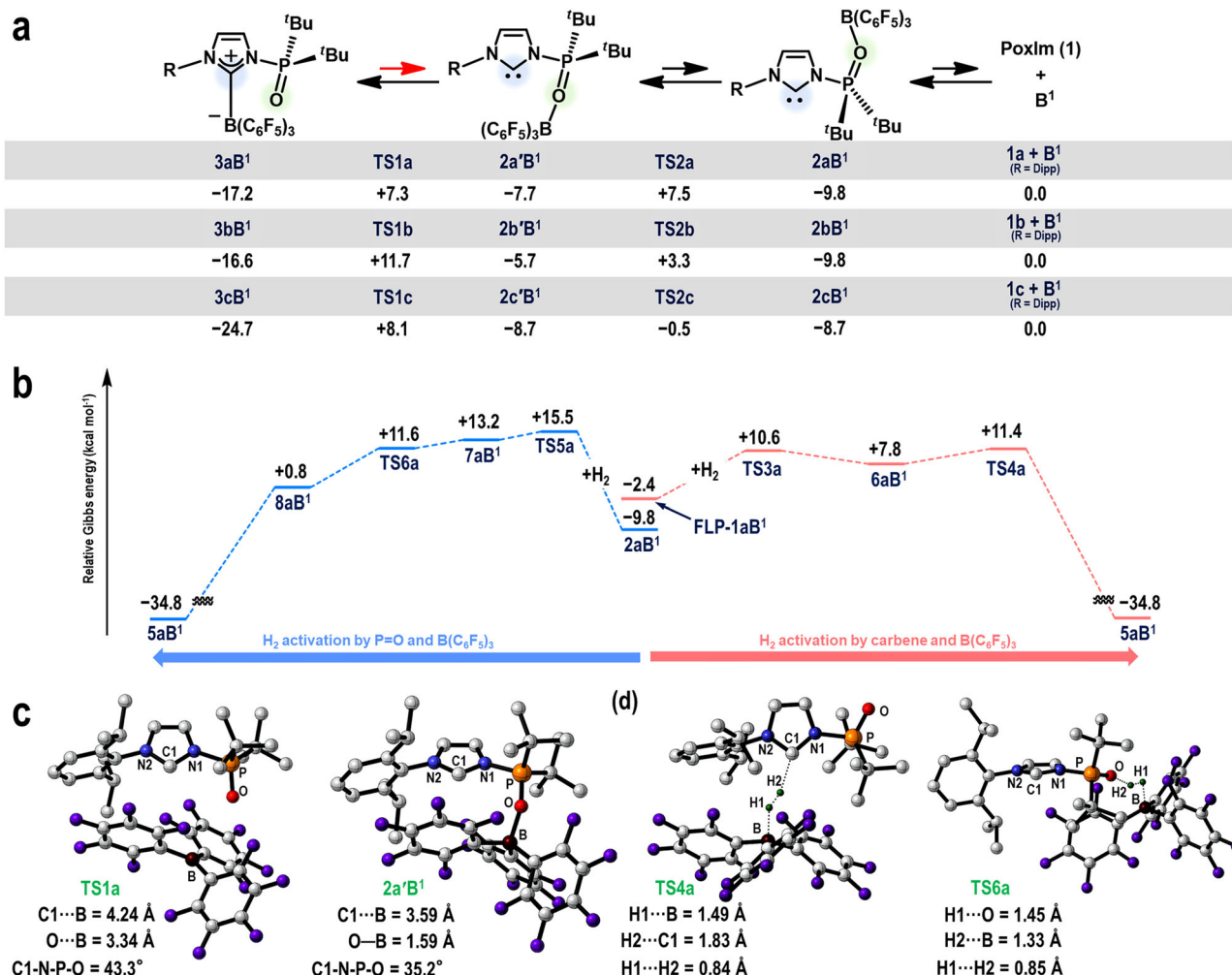


Fig. 5 Theoretical studies. The relative Gibbs energies [kcal mol⁻¹] are shown with respect to each [1 + B¹], calculated at the ω B97X-D/6-311G(d,p), PCM (DCE)// ω B97X-D/6-31G(d,p) (for H₂) and 6-31G(d) (for all other atoms) level of theory (298.15 K, 1 atm). **a** Proposed mechanism for the regeneration of [1 + B¹] from the carbene–borane complexes 3aB¹–3cB¹. **b** Proposed mechanism for the heterolytic cleavage of H₂, enabled by the phosphinoyl oxygen and B(C₆F₅)₃ moieties (left) or by the carbene and B(C₆F₅)₃ moieties (right). **c** DFT-optimized molecular structures for TS1a and 2aB¹. **d** DFT-optimized molecular structures for TS4a and TS6a.

conformational isomerization in the regulation of the reactivity of shelf-stable but external-stimuli-responsive Lewis acid-base adducts by multifunctional Lewis bases.

Methods

Synthesis of 3aB². PoxIm 1a (154.8 mg, 0.40 mmol) and B(p-HC₆F₄)₃ (B²) (183.4 mg, 0.40 mmol) were mixed in toluene (10 mL) at room temperature to furnish the yellow solution. Stirring this mixture for 4 h resulted into the precipitation of a white solid that was collected via removal of the supernatant solution. The obtained solid was washed with hexane (5 mL) and dried in vacuo to afford 3aB² as a white solid (230.2 mg, 0.27 mmol, 68%). A single crystal suitable for X-ray diffraction analysis was prepared by recrystallization from CH₂Cl₂/hexane at -30 °C.

Synthesis of 5aB². A solution of 3aB² (51.6 mg, 0.06 mmol) in CH₂Cl₂ (3 mL) was transferred into an autoclave reactor, which was then pressurized with H₂ (5 atm). Subsequently, the reaction mixture was stirred at 60 °C for 4 h, before the solvent was removed in vacuo to give 5aB² as a white solid (51.8 mg, 0.06 mmol, >99%). A single crystal suitable for X-ray diffraction analysis was prepared by recrystallization from THF/hexane at -30 °C.

Reaction between 1a and B² giving 2aB². A solution of 1a (7.4 mg, 0.02 mmol) and B² (9.3 mg, 0.02 mmol) in CD₂Cl₂ (0.5 mL) was prepared at -30 °C and then transferred into a J. Young NMR tube. The quantitative formation of 2aB² was confirmed at -90 °C by ¹H, ¹³C, ¹⁹F, and ³¹P NMR analysis (Supplementary

Figs. 5–8). A single crystal suitable for X-ray diffraction analysis was prepared by recrystallization from toluene/hexane at -30 °C.

Data availability

The datasets generated during and/or analyzed during the current study are available from the corresponding author on reasonable request. Details for the preparation of materials, monitoring the reactions (Supplementary Figs. 5–30), and theoretical analysis/discussion are provided in the Supplementary Information. Compound characterization data including ESI-MS, elementary analysis, and SC-XRD data are also available in the Supplementary Information. NMR spectra for the isolated compounds are provided in the Supplementary Information. Results of the AIM analysis for TS1a are provided in Supplementary Fig. 37, as well as Supplementary Data 1. Metrical data for the solid-state structures are available from the Cambridge Crystallographic Data Centre (CCDC) under reference numbers CCDC2072358 (3aB²), 2072359 (5aB²), 2072360 (2aB²), and 2072638 ([1a–H][HO(B²)₂]) (Supplementary Data 2–5). These data can be obtained free of charge from the CCDC via www.ccdc.cam.ac.uk/data_request/cif.

Received: 19 May 2021; Accepted: 6 September 2021;
Published online: 27 September 2021

References

- Stephan, D. W. & Erker, G. Frustrated Lewis pairs: metal-free hydrogen activation and more. *Angew. Chem. Int. Ed.* **49**, 46–76 (2010).

2. Paradies, J. Frustrated Lewis pair catalyzed hydrogenations. *Synlett* **24**, 777–780 (2013).
3. Feng, X. & Du, H. Metal-free asymmetric hydrogenation and hydrosilylation catalyzed by frustrated Lewis pairs. *Tetrahedron Lett.* **55**, 6959–6964 (2014).
4. Stephan, D. W. & Erker, G. Frustrated Lewis pair chemistry: development and perspectives. *Angew. Chem. Int. Ed.* **54**, 6400–6441 (2015).
5. Weicker, S. A. & Stephan, D. W. Main group Lewis acids in frustrated Lewis pair chemistry: beyond electrophilic boranes. *Bull. Chem. Soc. Jpn.* **88**, 1003–1016 (2015).
6. Scott, D. J., Fuchter, M. J. & Ashley, A. E. Designing effective ‘frustrated Lewis pair’ hydrogenation catalysts. *Chem. Soc. Rev.* **46**, 5689–5700 (2017).
7. Fasano, V. & Ingleson, M. J. Recent advances in water-tolerance in frustrated Lewis pair chemistry. *Synthesis* **50**, 1783–1795 (2018).
8. Jupp, A. R. & Stephan, D. W. New directions for frustrated Lewis pair chemistry. *Trends Chem.* **1**, 35–48 (2019).
9. Hoshimoto, Y. & Ogoshi, S. Triarylborane-catalyzed reductive *N*-alkylation of amines: a perspective. *ACS Catal.* **9**, 5439–5444 (2019).
10. Pan, T. & Liu, J. Catalysts encapsulated in molecular machines. *ChemPhysChem* **17**, 1752–1758 (2016).
11. Cheng, C. & Stoddart, J. F. Wholly synthetic molecular machines. *ChemPhysChem* **17**, 1780–1793 (2016).
12. Kassem, S. et al. Artificial molecular motors. *Chem. Soc. Rev.* **46**, 2592–2621 (2017).
13. Findlay, J. A. & Crowley, J. D. Functional nanomachines: recent advances in synthetic molecular machinery. *Tetrahedron Lett.* **59**, 334–346 (2018).
14. Rokob, T. A., Hamza, A., Stirling, A. & Pápai, I. On the mechanism of $B(C_6F_5)_3$ -catalyzed direct hydrogenation of imines: inherent and thermally induced frustration. *J. Am. Chem. Soc.* **131**, 2029–2036 (2009).
15. Jiang, C., Blacque, O., Fox, T. & Berke, H. Heterolytic cleavage of H_2 by frustrated B/N Lewis pairs. *Organometallics* **30**, 2117–2124 (2011).
16. Herrington, T. J. et al. Bypassing a highly unstable frustrated Lewis pair: dihydrogen cleavage by a thermally robust silylium-phosphine adduct. *Chem. Commun.* **50**, 12753 (2014).
17. Hoshimoto, Y., Kinoshita, T., Ohashi, M. & Ogoshi, S. A strategy to control the reactivation of frustrated Lewis pairs from shelf-stable carbene borane complexes. *Angew. Chem. Int. Ed.* **54**, 11666–11671 (2015).
18. Wu, L., Chitnis, S. S., Jiao, H., Annibale, V. T. & Manners, I. Non-metal-catalyzed heterodehydrocoupling of phosphines and hydrosilanes: mechanistic studies of $B(C_6F_5)_3$ -mediated formation of P–Si bonds. *J. Am. Chem. Soc.* **139**, 16780–16790 (2017).
19. Han, Y., Zhang, S., He, J. & Zhang, Y. Switchable C–H silylation of indoles catalyzed by a thermally induced frustrated Lewis pair. *ACS Catal.* **8**, 8765–8773 (2018).
20. Wang, X., Kehr, G., Daniliuc, C. G. & Erker, G. Internal adduct formation of active intramolecular C_4 -bridged frustrated phosphane/borane Lewis pairs. *J. Am. Chem. Soc.* **136**, 3293–3303 (2014).
21. Holtrichter-Rößmann, T. et al. Generation of weakly bound Al–N Lewis pairs by hydroalumination of ynamines and the activation of small molecules: phenylethyne and dicyclohexylcarbodiimide. *Organometallics* **31**, 3272–3283 (2012).
22. Mömmling, C. M., Kehr, G., Wibbeling, B., Fröhlich, R. & Erker, G. Addition reactions to the intramolecular mesityl₂P–CH₂–CH₂– $B(C_6F_5)_2$ frustrated Lewis pair. *Dalton Trans.* **39**, 7556–7564 (2010).
23. Spies, P. et al. Metal-free dihydrogen activation chemistry: structural and dynamic features of intramolecular P/B pairs. *Dalton Trans.* 1534–1541 <https://pubs.rsc.org/en/content/articlelanding/2009/dt/b815832k> (2009).
24. Spies, P. et al. Rapid intramolecular heterolytic dihydrogen activation by a four-membered heterocyclic phosphane-borane adduct. *Chem. Commun.* 5072–5074 <https://pubs.rsc.org/en/content/articlelanding/2007/cc/b710475h> (2007).
25. Kolychev, E. L. et al. Reactivity of a frustrated Lewis pair and small-molecule activation by an isolable arduengo carbene– $B\{3,5-(CF_3)_2C_6H_3\}_3$ complex. *Chem. -Eur. J.* **18**, 16938–16946 (2012).
26. Geier, S. J. & Stephan, D. W. Lutidine/ $B(C_6F_5)_3$: at the boundary of classical and frustrated Lewis pair reactivity. *J. Am. Chem. Soc.* **131**, 3476–3477 (2009).
27. Hazra, S., Hoshimoto, Y. & Ogoshi, S. *N*-Phosphine oxide-substituted imidazolylidenes (poxims): multifunctional multipurpose carbenes. *Chem. -Eur. J.* **23**, 15238–15243 (2017).
28. Hoshimoto, Y. & Ogoshi, S. Development of metal complexes equipped with structurally flexible carbenes. *Bull. Chem. Soc. Jpn.* **94**, 327–338 (2021).
29. Asada, T., Hoshimoto, Y., Kawakita, T., Kinoshita, T. & Ogoshi, S. Axial chirality around N–P bonds induced by complexation between $E(C_6F_5)_3$ (*E* = B, Al) and an *N*-phosphine oxide-substituted imidazolylidene: a key intermediate in the catalytic phosphinoylation of CO_2 . *J. Org. Chem.* **85**, 14333–14341 (2020).
30. Asada, T., Hoshimoto, Y. & Ogoshi, S. Rotation-triggered transmetalation on a heterobimetallic Cu/Al *N*-phosphine-oxide-substituted imidazolylidene complex. *J. Am. Chem. Soc.* **142**, 9772–9784 (2020).
31. Fan, L., Jupp, A. R. & Stephan, D. W. Remote stereochemistry of a frustrated Lewis pair provides thermal and photochemical control of reactivity. *J. Am. Chem. Soc.* **140**, 8119–8123 (2018).
32. Anslyn, E. V. & Dougherty, D. A. *Modern Physical Organic Chemistry* (University Science Books, 2006).
33. Bader, R. F. W. Ed. *Atoms in Molecules. A Quantum Theory* (Cambridge University Press, 1991).
34. Bader, R. F. W. & Stephens, M. E. Spatial localization of the electronic pair and number distributions in molecules. *J. Am. Chem. Soc.* **97**, 7391–7399 (1975).
35. Chase, P. A. & Stephan, D. W. Hydrogen and amine activation by a frustrated Lewis pair of a bulky *N*-heterocyclic carbene and $B(C_6F_5)_3$. *Angew. Chem. Int. Ed.* **47**, 7433–7437 (2008).
36. Holschumacher, D., Bannenberg, T., Hrib, C. G., Jones, P. G. & Tamm, M. Heterolytic dihydrogen activation by a frustrated carbene–borane Lewis pair. *Angew. Chem. Int. Ed.* **47**, 7428–7432 (2008).
37. Stepen, A. J., Bursch, M., Grimme, S., Stephan, D. W. & Paradies, J. Electrophilic phosphonium cation-mediated phosphane oxide reduction using oxalyl chloride and hydrogen. *Angew. Chem. Int. Ed.* **57**, 15253–15256 (2018).

Acknowledgements

This work was supported by Grants-in-Aid for Young Scientists (JSPS KAKENHI grants JP15K17824 and JP18K14219), Grants-in Aid for Scientific Research on Innovative Areas “Stimuli-responsive Chemical Species (JSPS KAKENHI grant JP15H00943)” and “Precisely Designed Catalysts with Customized Scaffolding (JSPS KAKENHI grants JP15H05803 and 15H05805),” and the Environment Research and Technology Development Fund (No. 1RF-2101) of the Environmental Restoration and Conservation Agency of Japan. Y.H. expresses his special thanks to Prof. Dr. T. Sasamori (University of Tsukuba) for valuable suggestions on this work. T.K. expresses his special thanks to a Grant-in-Aid for JSPS Fellows. M.R. and J.H. appreciate support from the Integrated Research Consortium on Chemical Sciences. A part of the computational work was performed at RCCS in Okazaki, Japan. A part of the study was supported by the Cooperative Research Program of Institute for Catalysis, Hokkaido University. S.O. would like to dedicate this work to Prof. Dr. Christian Bruneau.

Author contributions

This work was conceptualized and directed by Y.H. with the support of J.H. and S.O. M.S. and T.K. performed the experiments, while Y.H., M.S. and T.K. analyzed these data. M.O., M.R. and J.H. performed the computational analysis. The manuscript was prepared by Y.H. supported by discussions with all the other authors.

Competing interests

The authors declare no competing interests.

Additional information

Supplementary information The online version contains supplementary material available at <https://doi.org/10.1038/s42004-021-00576-1>.

Correspondence and requests for materials should be addressed to Yoichi Hoshimoto, Jun-ya Hasegawa or Senuke Ogoshi.

Peer review information *Communications Chemistry* thanks the anonymous reviewers for their contribution to the peer review of this work. Peer reviewer reports are available.

Reprints and permission information is available at <http://www.nature.com/reprints>

Publisher's note Springer Nature remains neutral with regard to jurisdictional claims in published maps and institutional affiliations.



Open Access This article is licensed under a Creative Commons Attribution 4.0 International License, which permits use, sharing, adaptation, distribution and reproduction in any medium or format, as long as you give appropriate credit to the original author(s) and the source, provide a link to the Creative Commons license, and indicate if changes were made. The images or other third party material in this article are included in the article's Creative Commons license, unless indicated otherwise in a credit line to the material. If material is not included in the article's Creative Commons license and your intended use is not permitted by statutory regulation or exceeds the permitted use, you will need to obtain permission directly from the copyright holder. To view a copy of this license, visit <http://creativecommons.org/licenses/by/4.0/>.

© The Author(s) 2021